Source de-ghosting and directional designature using near-field derived airgun signatures

Neil Hargreaves, Rob Telling, Sergio Grion (Dolphin Geophysical)

We have shown in previous work that directional airgun far-field signatures can be derived from measurements made near to the guns through an inversion process, as an alternative to the commonly used iterative method. This approach has the advantage of being more accurate at low frequencies, since it more correctly handles the motion of the air bubble as it moves away from the gun.

In this paper we extend our approach to obtain shot-by-shot estimates of the array depth and sea-surface reflectivity as part of the signature estimation. Our method follows from the somewhat unexpected observation that the near-field data can contain a strong ghost component, such that there is a noticeable sensitivity of derived signatures to the depth and reflectivity parameters used for their computation.

We use the estimated array depth and reflectivity values to construct directional far-field signatures containing a shot-varying estimate of the sea-surface ghost, and demonstrate shot-by-shot source deghosting via their use for directional designature. Our results show that, compared to modelled signatures, our near-field derived signatures contain a more accurate representation of the bubble and ghost components of the signature, leading to an improved treatment of wavelet phase and amplitude at low frequencies.

Introduction

In past work (Hargreaves et al, 2015) we have described a method for deriving directional far-field signatures from near-gun recordings by a form of least-squares inversion. In our method, as in Ziolkowski et al (1982), we use data from hydrophones placed close to each gun in the array to obtain estimates of the "notional signature" of each gun, which is the signature obtained when the gun is firing in the pressure field generated by the other guns. Once notional signatures have been derived for a particular shot they can be used to construct far-field signatures at any desired direction away from the array.

Our method is an alternative to the commonly used iterative approach proposed by Parkes (1984). Its main advantage is that it is more accurate at low frequencies, since it correctly handles the motion of the air bubble as it moves away from the gun and towards other hydrophones. This is a problematic aspect of the iterative approach, which can cause low frequency inaccuracies, and in some circumstances instability in the solution.

A complication in both approaches is the need to model and remove the sea-surface ghost from the near-gun records. The notional signatures are by definition unghosted, but the records for each hydrophone contain contributions both from energy that has travelled directly to the hydrophone and also from energy that has travelled by reflection from the sea-surface. Accurate derivation of the notional signatures requires knowledge of the characteristics of the ghost – in the simplest case, the depth of the array and the sea-surface reflection coefficient.

Computation

We formulate the modelling from notional signatures to near-gun data by a time-frequency approach, in which phase shifts for arrival times are applied in the frequency domain and the amplitude scaling is applied in the time domain. Conceptually:

$$\mathbf{D} = \mathbf{S}\,\mathbf{A'}\,\mathbf{M}$$

where **D** represents the hydrophone data at all positions and all frequencies, **M** the notional signatures at all positions and all frequencies, and **A'** represents the process of using time-constant travel-path lengths to apply phase shifts for the travel times of the arrivals. **S** represents the process of inverse Fourier transformation of the direct arrival from each gun, multiplication by the inverse of time-varying distances, and then forward Fourier transformation. We obtain the notional signatures from a conjugate-gradients solution of the least-squares formulation $\mathbf{(S\,A')^{+}(S\,A')\,M = (S\,A')^{+}D}$, where $\mathbf{(S\,A')^{+}}$ is the adjoint of the forward operator.

Far-field signatures derived by this approach are a reasonable match to modelled signatures, providing they both use the same array depth and surface-reflectivity. Amplitude and phase spectra are broadly comparable but may show differences at low frequencies related to differences in the bubble and, as we will see in the next section, differences in their ghost content.

Derivation of ghost parameters from near-gun data

Figure 1 shows spectra for the notional signatures of one gun of an array derived at various shot locations along a test line, together with the spectrum of the equivalent modelled version of the notional signature. We note that whilst the spectrum of the modelled signature is smooth at high frequencies the derived signatures contain features which are found to vary noticeably when the depth and reflectivity values used for the computation are changed. We interpret these as the residual of the ghosting in the near-gun records.

We might expect that spherical spreading would cause the ghosting to be relatively weak, since the ghost arrivals have substantially longer path lengths than the direct arrivals. However, modelling

studies show that constructive addition of the ghost arrivals can cause the net ghosting to be comparable in amplitude to the direct arrivals. Although the ghost path lengths are greater than those of the direct arrivals, they have less variation, and there is a tendency towards greater constructive addition amongst the ghost arrivals. If we view the ghosting as being from a set of virtual sources above the water surface, we could say that there is a greater degree of "wavefront healing" in the ghosting compared to the direct arrival.

We can use this behavior to estimate a ghost depth and reflectivity from notional signatures derived for a range of trial depth and reflectivity values. Figure 2 shows that the residual error in a straight line fit to the high-frequency portion of their spectra has a well-defined minimum at the depth and reflectivity values that best match the field conditions. There is a sharp minimum versus depth and a broader minimum versus reflectivity, with the depth minimum sitting at approximately the same position for different reflectivity values.

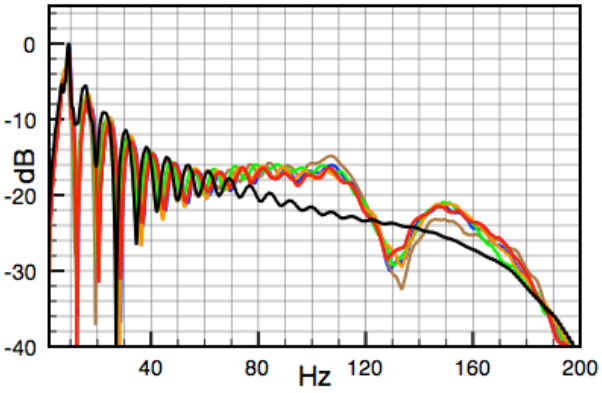

Figure 1. In colour, spectra for the notional signatures of one gun of an array for various shot locations, derived from near-gun records using an assumed array depth and sea-surface reflectivity. In black, Nucleus™ modelled notional signature for the equivalent gun of the array. Note the features at high frequencies in the derived spectra, which are related to the ghosting in the near-gun recordings.

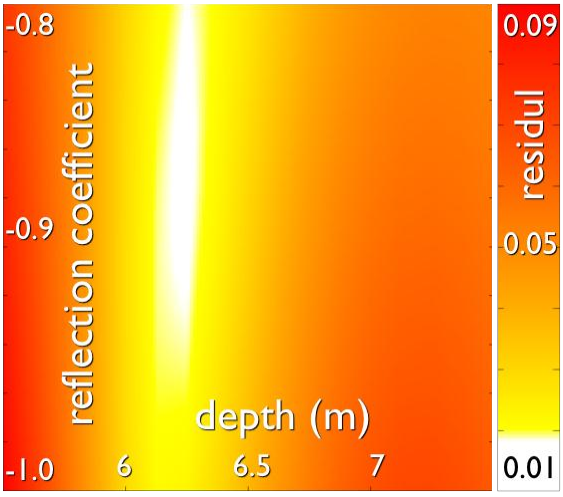

Figure 2. The residual error for a straight line fit to the high-frequency logarithmic spectra of derived notional signatures, for a range of source depths and surface reflectivity. There is a minimum at the depth and reflectivity values that best model the ghosting in the near-gun records.

This leads to a two-pass strategy for obtaining the optimum depth and reflectivity values. The depth value is obtained by a search over depth at a fixed reflectivity value, and the reflectivity is then obtained by a subsequent search over reflectivity at that depth. Interestingly, this is similar to the kurtosis optimisation problem for receiver-side ghosting (Grion et al, 2015), where the objective function has a similar behaviour and ghost delay-time and surface reflectivity can be obtained by a similar two-pass approach.

Figure 3 shows the spectra of notional signatures equivalent to those in Figure 1, but with the depth and reflectivity values for the computation being derived by this approach; there is a substantial reduction in the residual ghosting.

Additionally, depth and reflectivity values can be obtained on a shot-by-shot basis, and Figure 4 shows estimated depths and reflectivity values obtained from near-gun data for 500 consecutive shots from a test line.

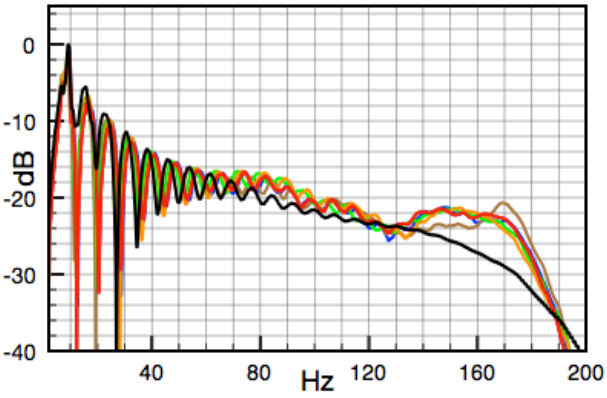

Figure 3. Repeat of the spectra of Figure 1, for notional signatures derived using data-estimated depths and reflectivity values as shown. This substantially reduces the residual ghosting.

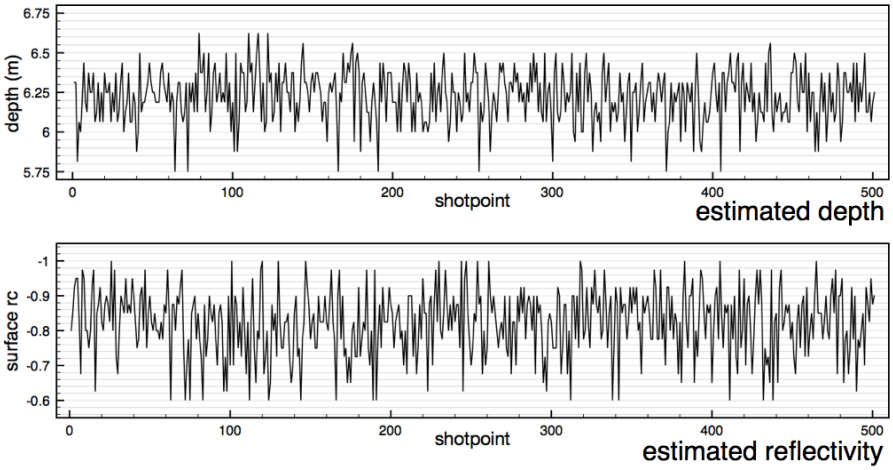

Figure 4. Estimated depth and reflectivity values for 500 consecutive shots of a test line. Note the rapid fluctuation of the values; this is consistent with the behaviour seen in directly measured far-field signatures.

If we assume that the depth and reflectivity that match the ghosting in the near-gun data are also a valid representation of the far-field ghost then we can construct directional, shot-by-shot, estimates of the source far-field ghost from these values. Including this ghost in far-field signatures derived from notional signatures allows directional shot-by-shot de-ghosting to be performed as part of signature deconvolution processing.

Application – directional de-ghosting and designature

In Figures 5 and 6 we compare the result of directional designature and de-ghosting using near-gun derived shot-dependent signatures and ghosts versus equivalent results obtained using a modelled signature with a fixed, assumed, ghost depth and sea-surface reflectivity.

Figure 5(a) shows an input unprocessed shot gather from a North Sea dataset. The ghosted bubble pulse of the signature generates the low frequency linear events in the display that follow the water-bottom arrival. These arrivals have a complicated range of departure angles from the source array and require directional designature and de-ghosting to remove them. They are present in all of the events throughout the data, but are most prominent in the case of the water-bottom arrival because of its relative strength compared to the other events.

Figure 5(b) is the result of applying directional designature and de-ghosting to this gather using modelled signatures and an assumed ghost. The processing quite successfully removes a significant amount of the bubble component, but there is still a residue of low frequency bubble-related energy in the data, as indicated by the arrow in Figure 5(b). In Figure 5(c) we see that this energy is better attenuated when using the near-field derived signatures and ghosting. The low-frequency spectra of the data shown in Figure 5(d) also confirm this result. The peaks in the spectrum here are related to the bubble pulse, and again are better suppressed using the near-field derived signatures and ghost.

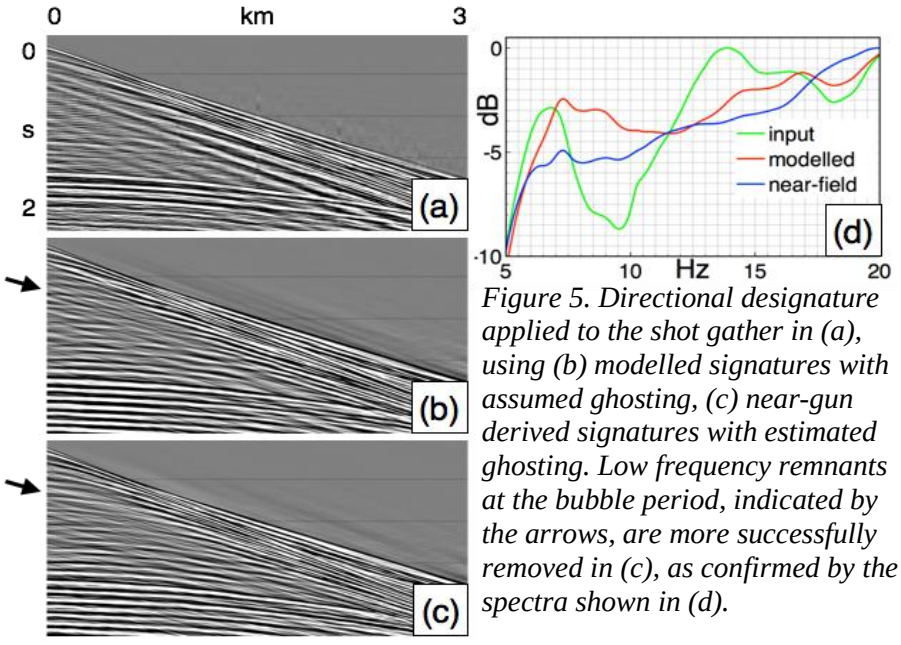

Figure 5. Directional designature applied to the shot gather in (a), using (b) modelled signatures with assumed ghosting, (c) near-gun derived signatures with estimated ghosting. Low frequency remnants at the bubble period, indicated by the arrows, are more successfully removed in (c), as confirmed by the spectra shown in (d).

Figure 6 shows portions of imaged data from the same survey, processed using modelled signatures and an assumed ghost in 6(a) and 6(c) and with near-gun derived signatures and ghosting in 6(b) and 6(d); the prominent event in these displays is Top Chalk. Figure 6(b) shows an improved treatment of the low-frequency component of the central portion of the seismic wavelet, with weakening of the white "halo" above the central event. Similarly in 6(d) the wavelet is more symmetric, without the low frequency tail that can be seen in 6(c). The weak features indicated by the arrow in 6(c) are the residual bubble pulse, and are also more successfully suppressed in 6(d).

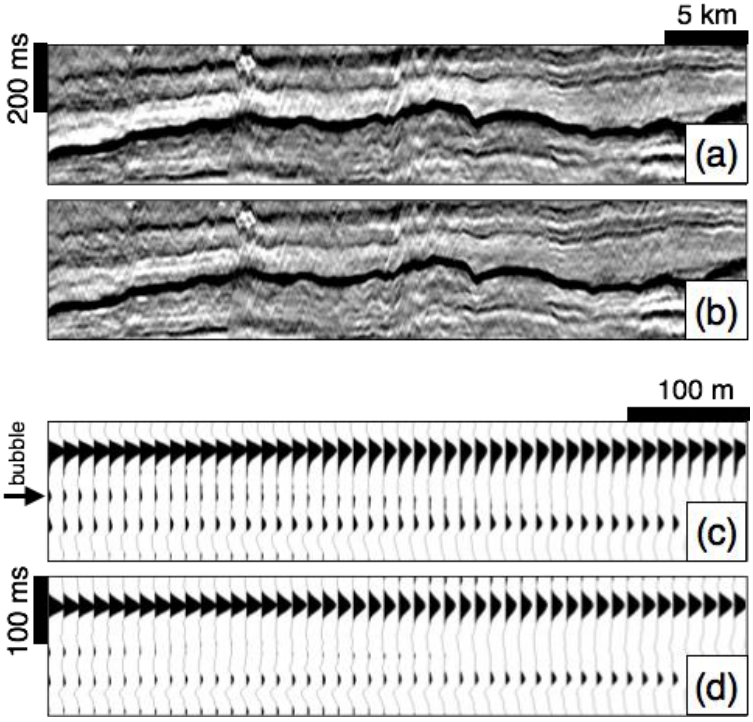

Figure 6. Directional designature applied to imaged data from a North Sea survey; (a) and (c) using modelled signatures, (b) and (d) using near-field derived signatures. (c) and (d) are close-ups from the left of the upper displays. Note the reduction of the low-frequency white "halo" in (b) and the improved symmetry of the central event plus suppression of the bubble in (d).

Conclusions

We have shown that features in notional signatures that are related to the ghosting in near-gun records can be used to derive shot-by-shot estimates of the array depth and reflectivity. We have used these to construct a shot-by-shot estimate of the directional far-field ghost and perform de-ghosting as part of directional source designature. We see improvements in the low frequency treatment of the wavelet when using near-gun derived signatures and ghosts, compared to using modelled signatures, in addition to improved removal of the signature bubble pulse.

Acknowledgements

The authors would like to thank the management of Dolphin Geophysical for permission to publish this paper, and in particular thank Gareth Williams for his support for this work. The real data example is courtesy of Dolphin's multi-client department.

References

Hargreaves N., Grion S. and Telling, R, [2015] Estimation of air-gun array signatures from near-gun measurements - least-squares inversion, bubble motion and error analysis, *SEG 2015* Expanded Abstracts, ACQ 5.1.

Grion, S., Telling, R., Barnes, J. [2015] De-ghosting by kurtosis maximization in practice, SEG 2015 Expanded Abstracts, 4605-4609.

Parkes G.E., A. Ziolkowski A., L. Hatton L. and Haugland T. [1984], The signature of an airgun array: computation from near-field measurements including interactions – practical considerations: *Geophysics*, **49,** 105–111.

Ziolkowski, A., Parkes, G.E, Hatton L and Haugland T. [1982] The signature of an air gun array: computation from near-field measurements including interactions: *Geophysics*, 47, 1413-1421.